Zinc Phthalocyanine *N*-Linked to Pyrroloperylenediimide Dyad: Significance of *N*-Connectivity in Modulating Photodynamics Towards Prolonging the Lifetime of Charge Separation

Chamari V. Ileperuma,[a] Jose Garcés-Garcés,[b] Ana M. Gutiérrez-Vílchez,[b] Ángela Sastre-Santos,[b] Fernando Fernández Lázaro*,[b] and Francis D'Souza*[a]

[a] C. V. Ileperuma and Prof. Dr. F. D'Souza
Department of Chemistry
University of North Texas at Denton
1155 Union Circle, #305070, Denton, TX 76203-5017, USA
Francis.DSouza@unt.edu
https://chemistry.unt.edu/people-node/francis-dsouza

[b] Dr. J. Garcés-Garcés, Dr. A. M. Gutiérrez-Vílchez, Prof. Dr. Á. Sastre-Santos, and Prof. Dr. F. Fernández-Lázaro
Área de Química Orgánica, Instituto de Bioingeniería
Universidad Miguel Hernández
Avda. de la Universidad s/n, 03203 Elche, Spain
fdofdez@umh.es; asastre@umh.es
http://quimicaorganica.umh.es

Abstract: A zinc phthalocyanine-pyrroloperylenediimide dyad connected through a nitrogen heteroatom (**PDI-N-ZnPc**) has been newly synthesized and characterized. Solvent polarity-dependent singlet-singlet energy transfer and electron transfer quenching were envisioned from absorption and steady-state fluorescence studies. Electrochemical and spectroelectrochemical studies enabled the assessment of the redox potential of the donor and acceptor entities, as well as the spectral characterization of the one-electron oxidation and reduction products. DFT studies were performed to investigate the geometry and electronic structure, as well as the role of *N*-connectivity in determining the relative orientation of the entities. Further, time-dependent DFT studies helped establish the different excited states responsible for promoting charge separation. An energy diagram was subsequently established to visualize different photo-physical events. Finally, femtosecond transient absorption spectral studies were performed in both nonpolar and polar solvents to observe energy and electron transfer events. The kinetic data were subsequently analyzed using global and target analyses. The persistence of the charge-separated state in the present dyad, compared with earlier reported ZnPc-PDI dyads featuring carbon-carbon connectivity, was the primary outcome of the present study, highlighting the role of heteroatom linkage in regulating electron transfer dynamics in donor-acceptor conjugates.

Keywords: zinc phthalocyanine, pyrroloperylenediimide, excited energy and electron transfer, DFT and TD-DFT, pump-probe transient spectroscopy

Introduction

One of the most important approaches in the development of artificial photosynthesis, organic photovoltaics (OPVs), and photo-driven charge-separation platforms is the design of π-conjugated donor–acceptor (D–A) molecular systems. Effective energy conversion requires both long-lived charge-separated (CS) states and rapid photoinduced charge separation, both of which have been made possible by covalently linked D–A dyads in particular.[1-5] From porphyrin–fullerene conjugates to phthalocyanine–perylenediimide hybrids, recent advances in this field have examined a wide variety of molecular architectures, revealing structure–property correlations that can be altered by electronic interaction and geometric alignment of components.[6-16]

Zinc phthalocyanine (ZnPc) and perylenediimide (PDI) units employed for these studies are particularly noteworthy because of their complementary optical characteristics, reversible redox behavior, and photostability. These characteristics make them perfect candidates for constructing highly functional D–A dyads that can form effective and durable charge-separated states (CS).[17-20] The remarkable thermal, chemical, and photochemical stability of ZnPcs as electron donors, together with their structural resemblance to naturally occurring porphyrins, is widely known. The substantial absorption of these compounds in the visible spectrum, particularly in the red and near-IR regions, makes them appropriate for light-harvesting applications.[18-21] Conversely, in artificial photosynthetic complexes and optoelectronic devices, PDIs are among the most potent electron acceptors. They are advantageous due to their high electron affinity, excellent fluorescence quantum yields, and great chemical and thermal durability. Furthermore, PDIs enable broad spectral coverage due to their strong absorption in the visible spectrum, which is complementary to the ZnPc absorption window.[22,23]

In our previously reported study, two ZnPc–PDI-based dyads (**Dyad 1** and **Dyad 2**) were synthesized to assess the effect of molecular geometry on electronic interactions and energy transfer (Figure 1). The main difference between these dyads was the type and stiffness of the linking motifs, which affected the orbital overlap, dihedral angle, and donor–acceptor center-to-center distance (R_{cc}). With a relatively reduced dihedral angle (~54°), **Dyad 1** exhibited stronger orbital conjugation and improved D–A alignment. However, while having a slightly greater R_{cc}, **Dyad 2** showed a closer to perpendicular arrangement between the donor and acceptor moieties (~72°), leading to a lower effective electronic coupling and less favorable charge-separation dynamics. This comparative study highlighted the importance of directionality of conjugated orbitals and dihedral orientation in determining the charge-transfer efficiency in D-A systems, in addition to proximity or planarity.[11]

Here, we demonstrate the structural and functional benefits inherent in the molecular architecture of our recently developed **PDI-N-ZnPc** dyad by comparing it systematically with **Dyads 1** and **2** (see Figure 1). The novel dyad efficiently lowers R_{cc} and increases orbital overlap while preserving electrical asymmetry by incorporating a directly conjugated ZnPc–PDI linkage via a pyrrolic N

bridge. By demonstrating a quick photoinduced charge separation ($\tau_{CS} \approx$ 13–18 ps) and a significantly long-lived CS state (~297 ps), the ultrafast transient absorption kinetic data outperforms **Dyad 2** and gets close to **Dyad 1**'s optimal performance. High oscillator strengths and good energy-level alignment are confirmed by electrochemical and spectroscopic investigations backed by DFT analysis. These findings propose a design paradigm that enhances photoinduced charge-transfer processes by combining regulated conjugation, asymmetric electronic potential, and compact D–A geometry. The current findings on the **PDI-N-ZnPc** dyad provide a strong molecular foundation for developing solar energy conversion and next-generation optoelectronic technology.[1–23]

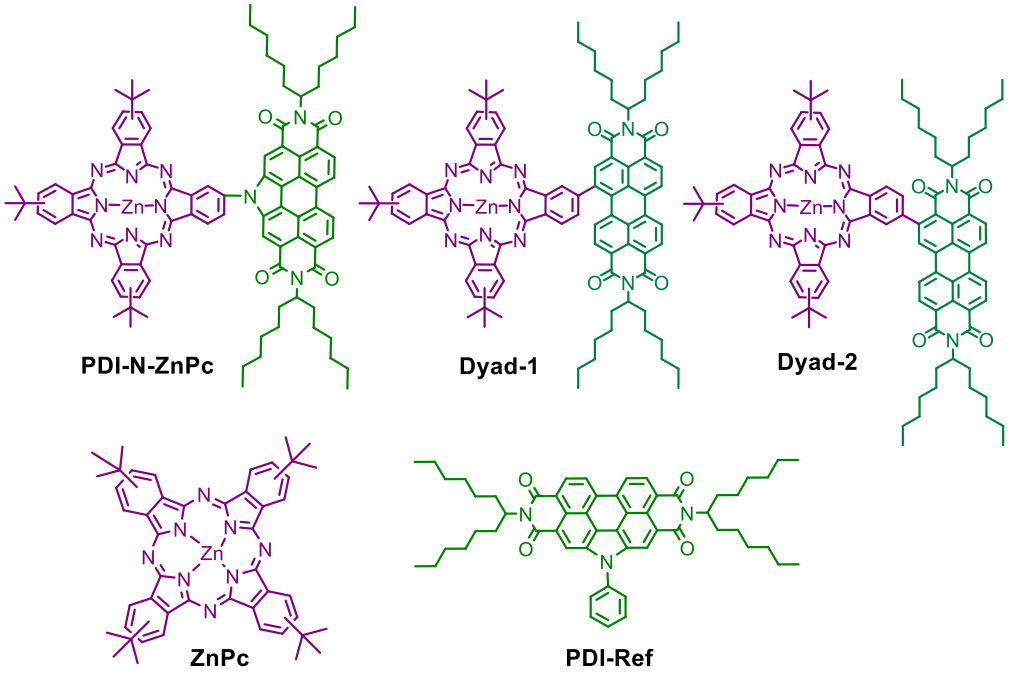

Figure 1. Chemical structures and abbreviations of the newly synthesized *N*-linked **PDI-N-ZnPc** dyad, along with previously reported directly linked ZnPc–PDI dyads (**Dyad 1** and **Dyad 2**),[11] and the control compounds used in the present study.

Results and Discussion

Synthesis

The synthesis of the target molecules, **PDI-N-ZnPc** and **PDI-Ref**, was carried out using the Buchwald-Hartwig coupling reaction[24] between **PDI-NH**[25] and either **Zn(IPc)**[26] or iodobenzene, yielding 84% and 6%, respectively. The reference phthalocyanine, **ZnPc**, was synthesized following a procedure described elsewhere.[27] Scheme 1 illustrates the synthesis route for both **PDI-N-ZnPc** and **PDI-Ref**. Final compounds were purified by automated chromatography and characterized by ^{1}H NMR, UV-vis, and FT-IR spectroscopies, as well as HR-

MALDI-ToF mass spectrometry (see Supporting Information, Figures S1-S9, for complete characterization data).

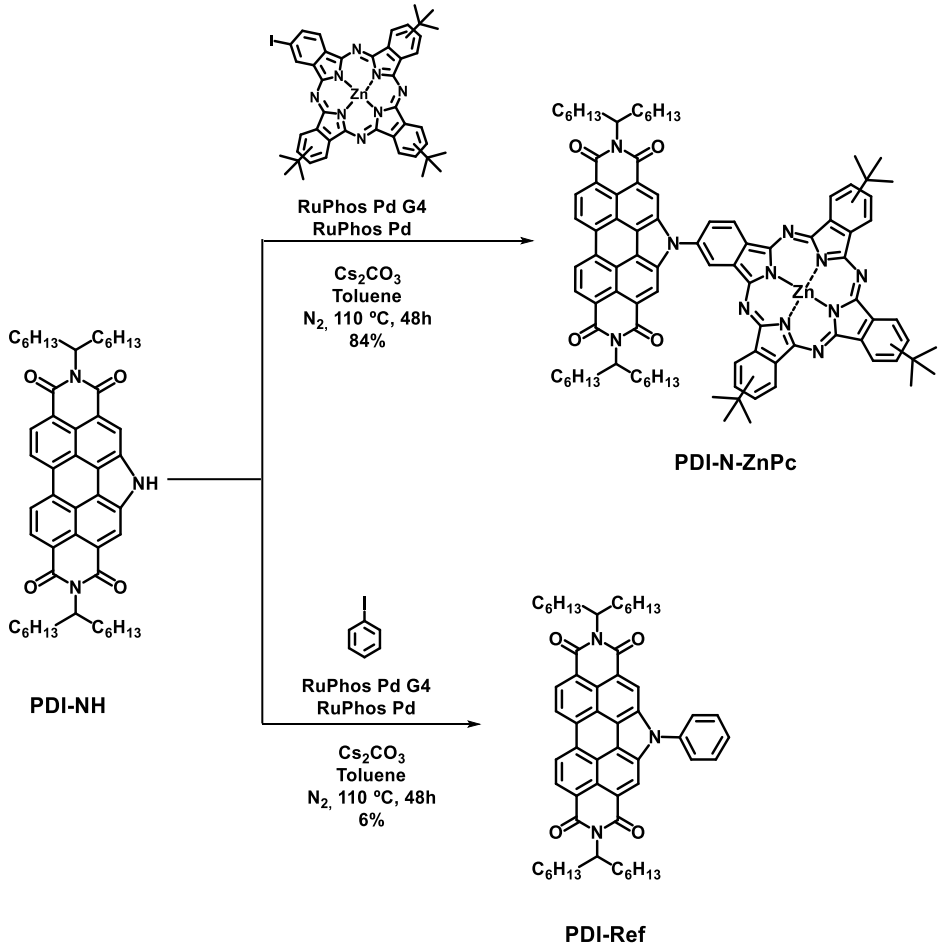

Scheme 1. Synthesis of **PDI-N-ZnPc** dyad and **PDI-Ref** compounds.

Absorption and fluorescence studies

The absorption spectra of the newly synthesized **PDI-N-ZnPc** dyad and reference compounds **PDI-Ref** and **ZnPc** in toluene are shown in Figure 2a. Three absorption peaks, corresponding to the π-π* transitions of perylenediimide, are observed at 459, 490, and 526 nm in the control compound **PDI-Ref**.[28-32] Along with two visible bands at 610 and 675 nm, control **ZnPc** exhibited a Soret band at 350 nm. The absorbance spectrum of the *N*-linked **PDI-N-ZnPc** dyad consisted of local wavelength maxima at 356, 490, 526, 610, 675, and 694 nm, resulting in a merged spectrum that reflects features from both donor and acceptor entities. However, all the key bands are broadened and bathochromically shifted in toluene and benzonitrile solvents (see Figure S10 in SI) compared to their reference spectra. Such spectral characteristics are indicative of ground-state electronic coupling and extended π-conjugation between the entities.[4] The emergence of an additional absorption peak at 694 nm in the **PDI-N-ZnPc** dyad, distinguished from the principal ZnPc Q-band at 675 nm, is ascribed to the alteration of the **ZnPc** electronic structure due to the

covalent linkage with the PDI unit. A second permitted transition could occur as a result of intramolecular splitting of the Q-band region caused by the *N*-linkage's ability to promote excitonic coupling between the donor and acceptor entities. On the other hand, two different Q-type absorptions might potentially result from the presence of two ground-state conformers that differ in their dihedral angles. In toluene, nearly gapless coverage of 300–750 nm of **PDI-N-ZnPc** dyad yielded a 35 % wider light harvesting range than **Dyad 1** or **Dyad 2** (Figure 2a).[11]

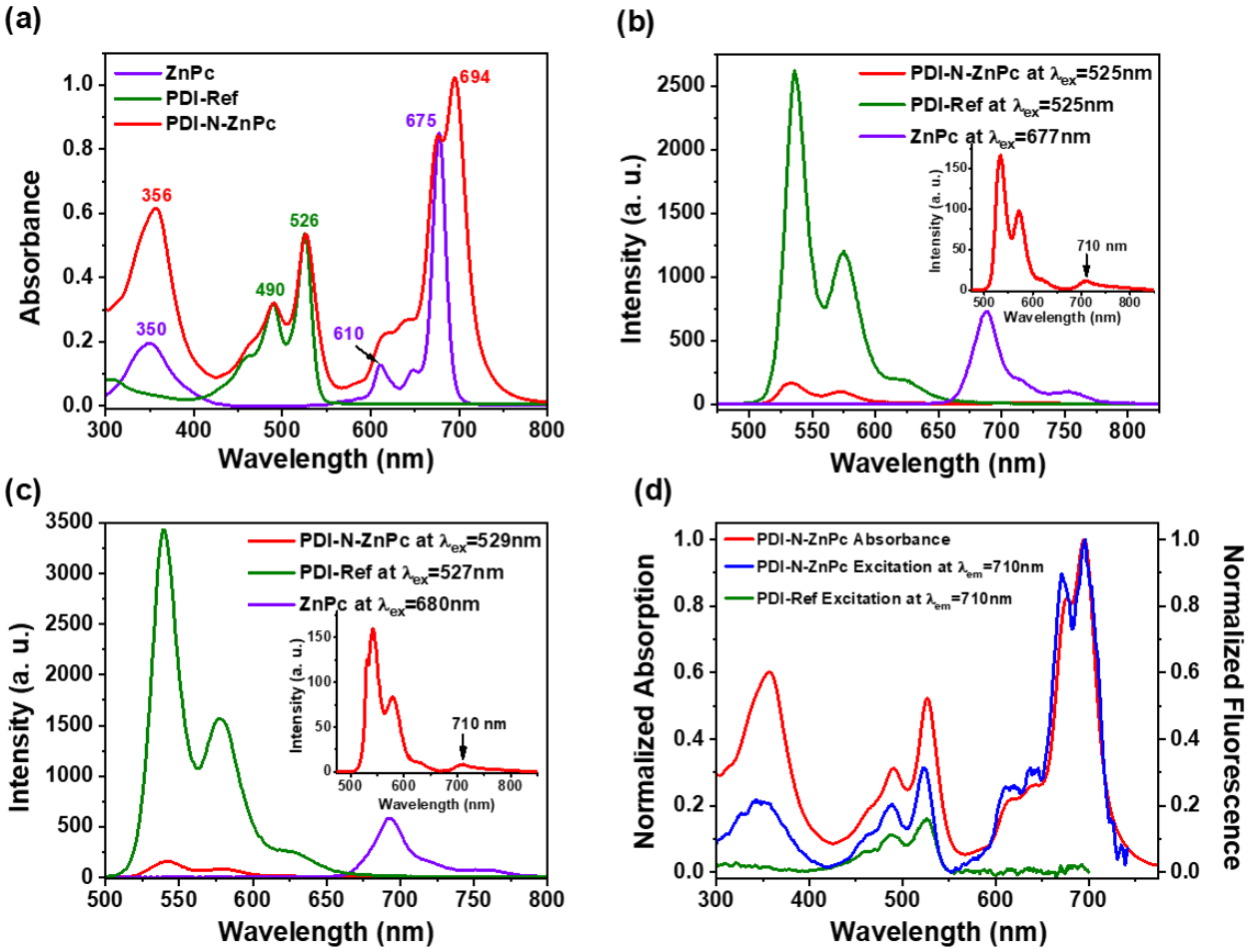

Figure 2. (a) Absorption spectra in toluene; emission spectra in (b) toluene and (c) benzonitrile, recorded upon excitation at the indicated absorption wavelengths for the **PDI-N-ZnPc** dyad, **ZnPc**, and **PDI-Ref**; (d) Excitation spectra of **PDI-N-ZnPc** dyad and **PDI-Ref** recorded by holding the emission monochromator to 710 nm (corresponding to the **ZnPc** reference emission peak), overlaid with the absorption spectrum of the dyad in toluene. The inset in (b) and (c) shows the enlarged emission spectra of **PDI-N-ZnPc** upon excitation at 525 nm.

The fluorescence spectra of the N-linked dyad and reference compounds in toluene and benzonitrile are shown in Figures 2b and 2c, respectively. Upon excitation in the PDI window (525-529 nm), the dyad's PDI emission was quenched by approximately 93% and 95% compared

to **PDI-Ref** in toluene and benzonitrile, respectively. This significant quenching suggests photoinduced electron or energy transfer from excited states to charge-separated states, likely via intramolecular interactions. However, previously reported **Dyad-1** and **Dyad-2** exhibited 92 and 84% fluorescence quenching efficiencies in benzonitrile, respectively. These reduced quenching efficiencies can be attributed to their corresponding higher dihedral angles (54.16° and 72.17°) and reduced orbital overlap between donor and acceptor entities compared to the N-linked dyad. The excitation spectrum of the **PDI-N-ZnPc** dyad was obtained by setting the emission monochromator to 710 nm, aligned with the peak emission maxima of **ZnPc**, while scanning the excitation wavelength (Figure 2d). Here, the excitation spectra reveal emission at 710 nm from the **PDI-N-ZnPc** dyad, with excitation scanning from 300 to 775 nm to identify the wavelengths that most efficiently induce emission. Under these circumstances, absorption peaks indicative of both **PDI** and **ZnPc** appeared suggesting the existence of singlet-singlet energy transfer.[33-35] Peaks corresponding to only **ZnPc** are anticipated from such an experiment in the absence of energy transfer.[33] An excitation transfer efficiency of around 45% for the dyad in toluene and approximately 34% in benzonitrile was calculated by recording the excitation spectra of equimolar **PDI-Ref** under equivalent experimental conditions. Not all photons absorbed by the PDI chromophore contribute to the observed **ZnPc** emission at 710 nm, which explains the increased absorption intensity of PDI (red) in the 425–550 nm range relative to its photoluminescence excitation (PLE) intensity (blue). This suggests that as an alternate deactivation pathway, the PDI unit may experience photoinduced electron transfer (discussed later) in addition to energy transfer to **ZnPc** following photoexcitation. The excitation spectrum of PDI-control was also recorded by holding the emission monochromator at 710 nm. Peaks corresponding to PDI but with relatively lesser intensity were observed (Figure 2d). The enhanced PDI peak intensity in the dyad suggests the occurrence of energy transfer to some extent.

Electrochemical and spectroelectrochemical studies

Electrochemical redox potentials are crucial for assessing the electron-donating and electron-accepting abilities of D-A conjugates and for evaluating the free energy changes associated with forward and reverse electron transfer processes. To probe these properties, electrochemical investigations were conducted in dichlorobenzene using 0.1 M tetrabutylammonium perchlorate ((TBA)ClO_4) as the supporting electrolyte. Since differential pulse voltammetry (DPV) provided accurate measurements of redox potentials, cyclic voltammetry (CV) was adopted to evaluate the reversibility of redox processes. Figure 3 depicts the DPVs, whereas Figure S11 in the SI presents the CVs for the novel dyad and reference compounds. Based on the CV data, most redox reactions were reversible within the experimental timescale, and the specific sites of electron transfer were identified by comparing the dyad's redox potentials with those of the references. The first oxidation and reduction of the **ZnPc** control occurred at 0.55 and -1.02 V (vs. Ag/AgCl), while reductions of **PDI-Ref** were at -0.66 and -0.93 V. In the **PDI-N-ZnPc** dyad, the first reduction at -0.64 coincides with the PDI reference. Conversely, the presence of the electronegative N-heteroatom of PDI reduced the feasibility of ZnPc oxidation, causing it to shift anodically by 170

mV and appear at 0.72 V. Furthermore, the facile oxidation of **ZnPc** and facile reduction of **PDI-Ref** confirmed their respective functions as electron donor and acceptor in this conjugate.[36-39]

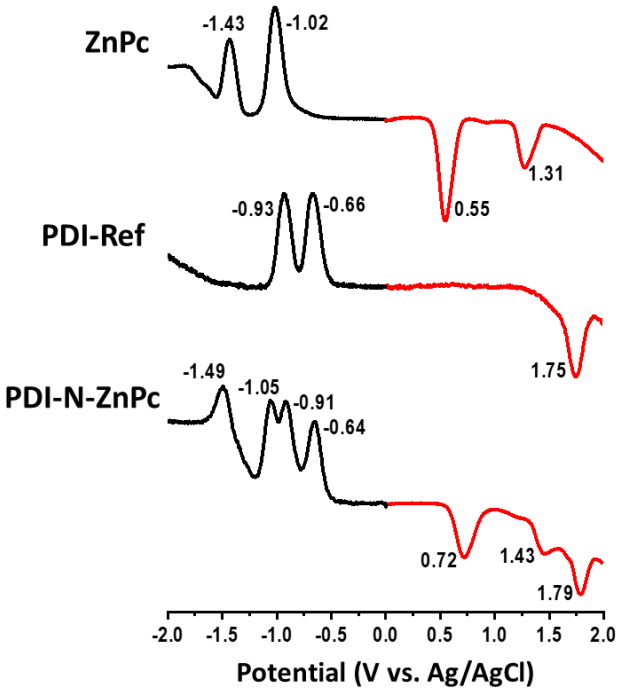

Figure 3. Differential pulse voltammograms of the indicated dyad and reference compounds in dichlorobenzene containing 0.1 M (TBA)ClO_4.

Next, spectroelectrochemical experiments were conducted using an optically transparent thin-layer electrochemical cell to analyze the oxidized and reduced species of both the reference compounds and the dyads, as these measurements are indispensable for identifying electron transfer products. Figure 4 depicts the spectral changes related to the first oxidation and first reduction of the dyad, whereas Figure S12 shows the spectral changes observed during the first reduction of **PDI-Ref** and the first oxidation of the **ZnPc**. The one-electron reduced PDI, $PDI^{\bullet-}$, revealed peaks at 700, 779, 848, and 930 nm (Figure S12a), while one-electron oxidized ZnPc, $ZnPc^{\bullet+}$ exhibited peaks at 442, 527, and 839 nm (Figure S12b). These peaks were observed in the dyad's one-electron reduced and one-electron oxidized products, affirming the site of electron transfer, i.e., the formation of $ZnPc^{\bullet+}$ during oxidation and the formation of $PDI^{\bullet-}$ during reduction, which electrochemical studies had previously determined.[28,40] However, structural and electrical changes resulting from electron uptake during the reduction of ZnPc (Figure S12c) result in a decrease in the Q-band absorbance around 700 nm of the neutral compound. This can be attributed to the blocking of HOMO → LUMO transition when **ZnPc** is reduced (producing $ZnPc^{\bullet-}$) because the additional electron occupies the π*-LUMO. The intensity of the Q-band at 700 nm decreased as a result of the π→π* transition being less intense. This is a typical occurrence in the electrochemistry of phthalocyanines and porphyrins, where redox reactions drastically change

optical characteristics.[41,42] These spectral features can later be utilized to identify the electron transfer products generated during photoexcitation in transient absorption spectroscopy studies.[25]

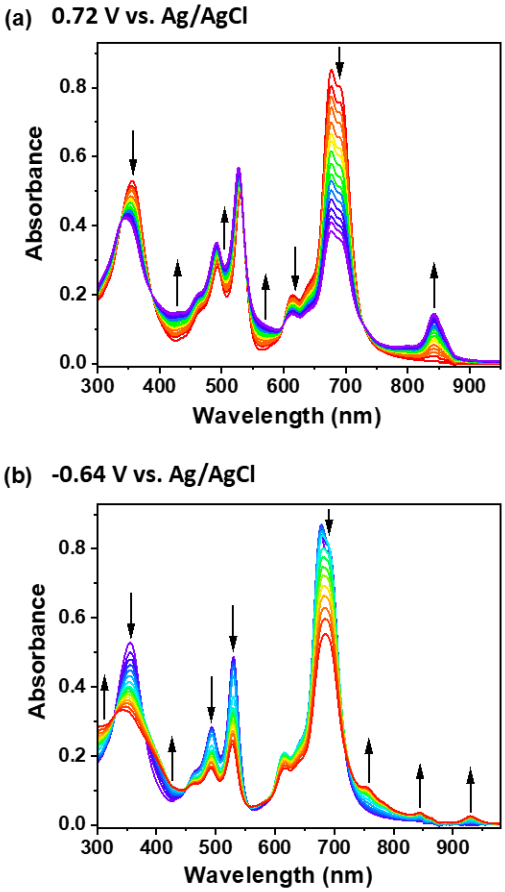

Figure 4. Spectral changes observed during (a) first oxidation and (b) first reduction of the **PDI-N-ZnPc** dyad in dichlorobenzene containing 0.2 M (TBA)ClO_4. Spectra were recorded until no additional spectral changes were observed at the applied potential.

Computational studies

To establish the donor and acceptor entities of the studied conjugates that contribute to the formation of charge-separated (CS) states in both the ground and excited states, density functional theory (DFT) and time-dependent DFT (TD-DFT) calculations were performed on **PDI-N-ZnPc**, **Dyad-1,** and **Dyad-2**. The dyads were geometrically optimized at the B3LYP/6-311+G(d,p) level in benzonitrile using the conductor-like polarizable continuum (CPCM) solvation model to a stationary point on the Born–Oppenheimer surface as implemented in Gaussian 16.[43] TD-DFT studies were performed at the same level in benzonitrile to obtain the excited-state properties of dyads. The GaussView 6 [44] program was loaded with the ground state charge density cube from DFT, the density cube for the relevant excited state, and the subtraction of the two cubes, to

visualize the difference between the ground state density and the excited state density, which is defined as "charge transfer".[45-49] Figure 5 illustrates the resulting optimized geometries, frontier HOMOs and LUMOs, as well as the location of charge transfer in the donor and acceptor parts of S_1 and S_5 excited states in these dyads. In all three dyads, the ZnPc and PDI entities appeared to be individually coplanar, covalently linked, fused-ring systems, creating dihedral angles that followed the trend: **PDI-N-ZnPc** (47.02°) < **Dyad-1** (54.16°) < **Dyad-2** (72.17°). Apart from that, HOMOs on ZnPc and LUMOs on PDI imply donor-acceptor properties of the two corresponding entities. However, the larger HOMO-LUMO gap (1.82 eV) in N-linked dyad suggests the charge transfer at a higher energy, which is also supported by the enhanced redox band gap in electrochemistry.

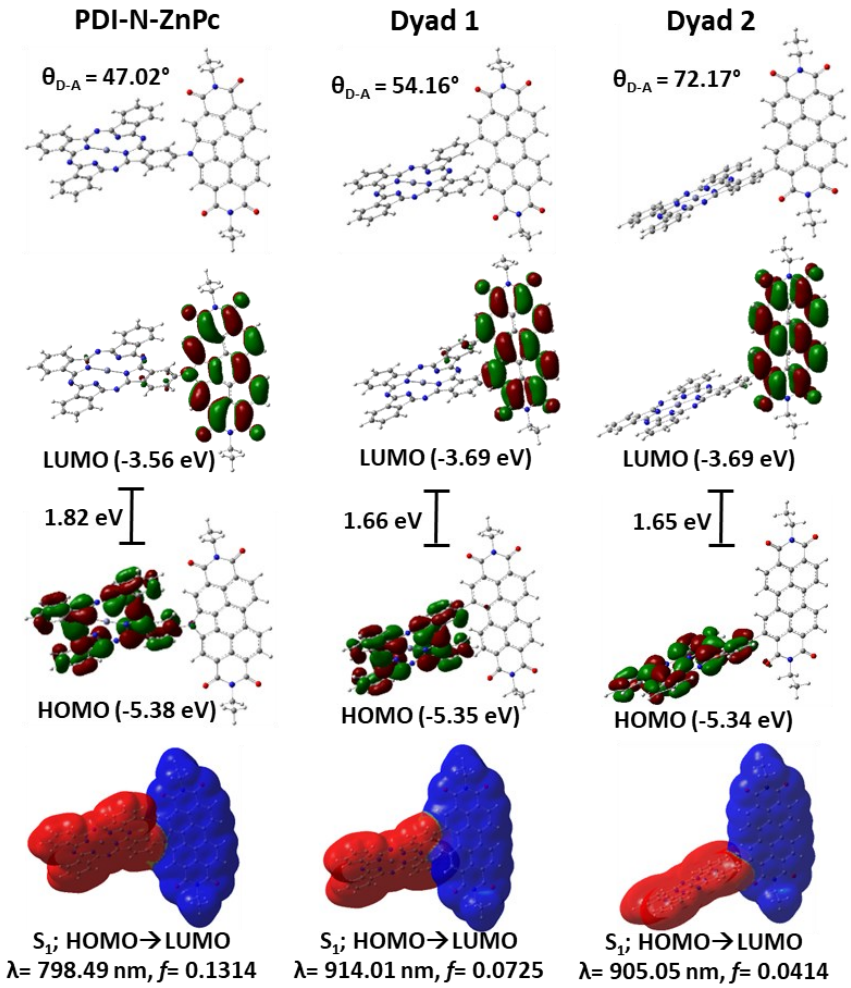

Figure 5. B3LYP/6-311+G (d,p) optimized geometries, frontier HOMOs and LUMOs with their corresponding energies, and TD-DFT calculated charge distribution from S_1 excited states of the indicated dyads. Electrostatic Potential Surface: Red=charge donor regions, Blue=charge acceptor regions (-5.000×10^{-6} V – 5.000×10^{-6} V). $\theta_{D\text{-}A}$ denotes the dihedral angle between donor and acceptor entities.

The S_1 excited state (HOMO → LUMO) charge-transfer transition in the novel dyad exhibits a blue shift of ~100 nm, accompanied by the highest oscillator strength (0.13), which is over threefold that of **Dyad-2** (0.04) and nearly double that of **Dyad-1** (0.07). This enhanced transition can be attributed to the N-pyrrolic bridge in the **PDI–N–ZnPc** dyad, which results in a shorter center-to-center distance and improved conjugation between the donor and acceptor entities. As a result, the charge-transfer energy gap increases, while electronic coupling is also strengthened. The last row in Figure 5 shows the charge difference map for the S_1 (HOMO → LUMO) transition for all the dyads. The formation of the $PDI^{\bullet-}$-N-$ZnPc^{\bullet+}$ charge-separated state is obvious in all three dyads. (see Figures S13 and S14 in SI for more details).

Energy level diagram

The Jablonski-type energy level diagram was implemented to visualize different photochemical events in the N-linked dyad, utilizing optical, redox, and theoretical structural data, as shown in Figure 6. The Gibbs free energy shift related to excited-state charge separation (CS) and dark charge recombination (CR) in toluene and benzonitrile was evaluated using Equations (1)–(2).[50,51]

$$-\Delta G_{CS} = \Delta E_{00} - (-\Delta G_{CR}) \quad (1)$$

$$-\Delta G_{CR} = E_{ox} - E_{red} + \Delta Gs \quad (2)$$

where ΔE_{00} represents the singlet state energy of the excited molecule. The first oxidation and reduction potentials are denoted by E_{ox} and E_{red}, respectively. Static Coulombic energy, as determined by the dielectric continuum model using Equation (3), is referred to as ΔG_S.

$$\Delta G_S = \frac{e^2}{4\Pi\varepsilon_0}\left[\left(\frac{1}{2R_D} + \frac{1}{2R_A}\right)\Delta\left(\frac{1}{\varepsilon_R}\right) - \frac{1}{R_{cc}\varepsilon_R}\right] \quad (3)$$

The dielectric constant of the solvent employed in photochemical and electrochemical studies and the permittivity of vacuum are denoted by the symbols ε_0 and ε_R, respectively. The center-to-center distance between the donor and acceptor entities of the newly synthesized dyad from the computed structure is represented by R_{cc}, while the symbols R_D and R_A stand for the radii of the electron donor and acceptor, respectively, as illustrated in Figures 5 and S13.

In addition to the fluorescence and intersystem crossing, the ^{1}PDI* produced by the dyad's excitation at 530 nm exhibits at least two deactivation pathways, i.e., charge separation and energy transfer (Figure 6). According to the previously discussed steady-state emission data, energy transfer has led to the generation of ^{1}ZnPc*. Direct excitation of ZnPc at its primary absorption wavelength at 680 nm could similarly produce the ^{1}ZnPc*state. ^{1}ZnPc* possesses adequate energy to generate charge separation that is thermodynamically feasible and leads to $PDI^{\bullet-}$-N-$ZnPc^{\bullet+}$ charge-separated state. Furthermore, it is noteworthy that both polar and non-polar solvents facilitate such a charge separation process. Though slightly higher in energy with respect to ^{3}PDI* and ^{3}ZnPc* (~1.00[40] and 1.26 eV[52], respectively), the charge-separated state's energy varies from

1.33 to 1.00 eV, corresponding to the solvent polarity. The charge-separated state may then either relax straight to the ground state or populate the triplet state of one of the entities.

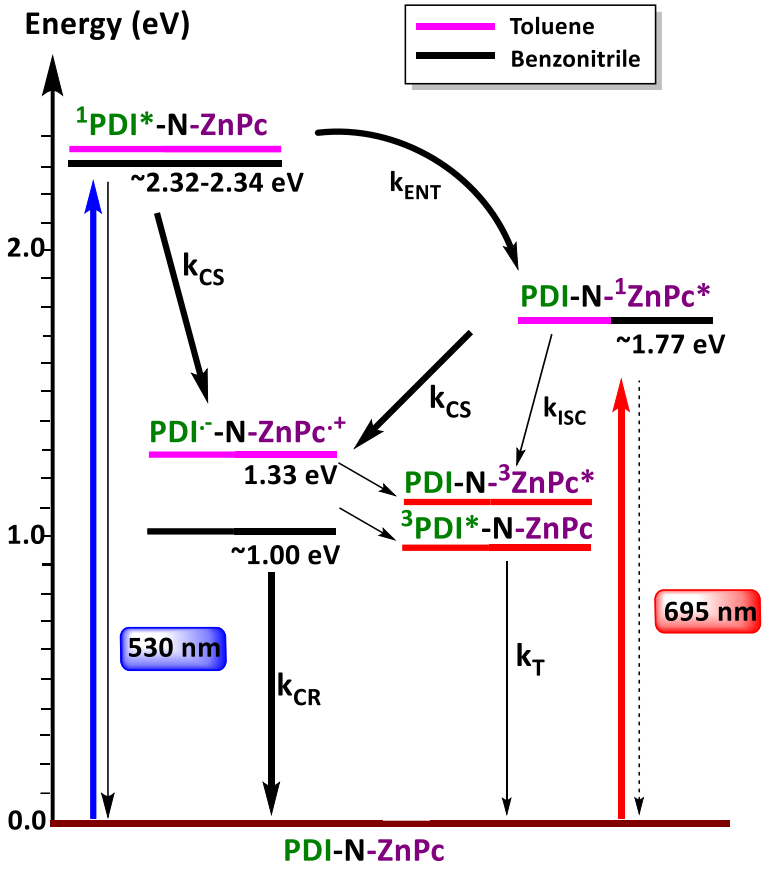

Figure 6. Energy level diagram depicting the different photochemical events occurring in **PDI-N-ZnPc** dyad in toluene and benzonitrile. The energies of different states were evaluated from spectral and electrochemical studies. ENT=singlet excited energy transfer, CS=charge separation, ISC = intersystem crossing, CR=charge recombination, T = decay of the triplet state. Thick arrows represent major photochemical events, while thin and dashed arrows represent minor photochemical events.

Femtosecond transient absorption, fs-TA studies

Subsequently, femtosecond transient absorption spectroscopy (fs-TA) was used to systematically investigate the existence of predicted photochemical events by selectively exciting the ZnPc at 680 nm and PDI at 530 nm in the conjugates, in toluene and benzonitrile. To determine the time constants of various photochemical events, the fs-TA data were then analyzed by constructing evolution-associated spectra (EAS) using GloTarAn analysis.[53-56] Figures S15 and S16 show the fs-TA spectra of **ZnPc** and **PDI-Ref** excited at 680 and 530 nm, along with their normalized EAS and population kinetics in toluene and benzonitrile, respectively. For the **PDI-Ref** shown in Figure S15b, excited state absorption (ESA) peaks at 454, 649, 768, and 944 nm indicate the instantaneous formation of the singlet excited state. Additionally, stimulated emission (SE) peaks at 582 nm and ground state bleach (GSB) peaks at 490 and 530 nm were observed. The SE and pump scattering

also contributed to the 530 nm peak. The 944 nm ESA peak differed from the 848 and 930 nm peaks of $PDI^{\bullet-}$ from the earlier discussed spectroelectrochemistry, although they are close in wavelength. Recovery of the negative peaks and decay of the positive peaks did not show new peaks corresponding to the ^{3}PDI* formation from intersystem crossing (ISC) within the monitoring window of 3.0 ns, suggesting that such a process is slow or that the absorptivity of ^{3}PDI* is relatively low. The normalized EAS and population kinetics from GloTarAn analysis yielded 2.21 and 2.45 ns singlet lifetimes in toluene (Figure S15) and benzonitrile (Figure S16), respectively. The ^{1}ZnPc* exhibited ESA peaks at 497, 572, 630, 735, 859, and 876 nm (Figure S15a), along with GSB peaks at 615 and 680 nm. The 680 nm peak was also caused by pump scattering and the SE peak at 710 nm. The GloTarAn analysis revealed that the ^{1}ZnPc* persisted for 2.98 and 2.61 ns in toluene and benzonitrile, respectively.

The fs-TA spectra for the **PDI-N-ZnPc** dyad in toluene, excited at 530 nm, which corresponds to PDI fragment, are illustrated in Figure 7a. Excitation transfer from ^{1}PDI* to ZnPc was demonstrated by earlier steady-state fluorescence analyses. The spectra exhibited minor characteristics of ^{1}PDI* at the earliest detectable delay time, such as the ESA peak at 769 nm, the SE peak at 580 nm, and the GSB peak at 490 and 569 nm (see spectrum at 487 fs in Figure S17a). The ESA peaks at 560 and 735 nm, which correspond to ^{1}ZnPc* (see spectrum at 765 fs), were formed by the rapid recovery and decay of the GSB and SE peaks, suggesting direct evidence of energy transfer in the dyad. The kinetic fitting at 687 nm, which corresponds to the **ZnPc** ground state bleaching region and exhibits negligible spectral overlap with PDI transitions, was used to calculate the energy transfer rate constant. Within error bounds, the rate constant obtained via GloTarAn analysis was moreover consistent with the kinetic trace. By fitting the time profile of the 687 nm peak, the rate of energy transfer (k_{EnT}) was determined to be 11.8×10^{10} s^{-1}, suggesting that ultrafast energy transfer occurred in the dyad (see Table S1 in SI). New peaks anticipated for the charge-separated state were generated by the immediate decay and recovery of the ESA peaks of the energy transfer product, ^{1}ZnPc* (see spectra at 299 ps). There were noticeable major peaks at 766 and 910 nm corresponding to $PDI^{\bullet-}$ and 558 and 855 nm corresponding to $ZnPc^{\bullet+}$. As shown in Figure 8a, comparable spectral characteristics have been identified, indicating the initial energy transfer and subsequent electron transfer events for the N-linked dyad in benzonitrile. Upon excitation at 532 nm, the initially formed ^{1}PDI* exhibited a faster recovery of the GSB peak at 493 nm and the SE peak at 569 nm, along with decay of the ESA peak at 645 nm (see the spectrum at 765 fs in Figure S18a). This was accompanied by a new set of peaks at 633, 735, and 880 nm in the spectrum at 1.23 ps corresponding to the ESA of ^{1}ZnPc*, thus confirming the occurrence of singlet-singlet energy transfer. By analyzing the time profile of the 686 nm peak, the rate of energy transfer, k_{EnT}, was calculated to be 8.99×10^{10} s^{-1}. Further, recovery of the ^{1}ZnPc* peaks was followed by another new set of peaks at 458, 570, 743, 850, and 930 nm, expected for the $(PDI\text{-}N)^{\bullet-}$-$ZnPc^{\bullet+}$ charge-separated state in the spectrum at 14.7 ps. The results tabulated in Table 1 suggest that electron transfer occurs at a higher rate of charge separation (k_{CS}) and a lower rate of charge recombination (k_{CR}) in toluene than in benzonitrile. As a result of this, toluene facilitates the long-lived charge-separated state by 752.26 ps compared to benzonitrile (187.17 ps).

The ability of ^{1}ZnPc* to facilitate electron transfer involving electron acceptor PDI in the **PDI-N-ZnPc** dyad was investigated by probing the electron transfer from directly excited ZnPc at 680 nm. The transient spectral properties of the dyad excited at 680 nm in toluene and benzonitrile are given in Figures 7b and 8b, respectively. The spectrum at 1.23 ps in Figure S17b and at 951 fs in

Figure S18b exhibited the expected ESA peaks at 471, 509, and 558 nm alongside the GSB peaks at 612 nm in both cases of the ^{1}ZnPc* generated by direct excitation within the first couple of ps. The decay and the recovery of these peaks revealed new peaks corresponding to (PDI-N)$^{\bullet-}$-ZnPc$^{\bullet+}$ formation. That is, PDI$^{\bullet-}$ peaks at the 756 and 912 nm range, and ZnPc$^{\bullet+}$ peaks in the ~570 and 855 nm were observed. These results provide evidence of charge separation from ^{1}ZnPc*. Rapid charge separation (11.77 ps) and prolonged charge recombination (2.93 ns) were detected in toluene, than that in benzonitrile (CS = 13.46 ps and CR = 251.49 ps). The signals corresponding to (PDI-N)$^{\bullet-}$-ZnPc$^{\bullet+}$ ion-pair persisted over 3 ns in toluene, the monitoring time window of our instrumental setup.

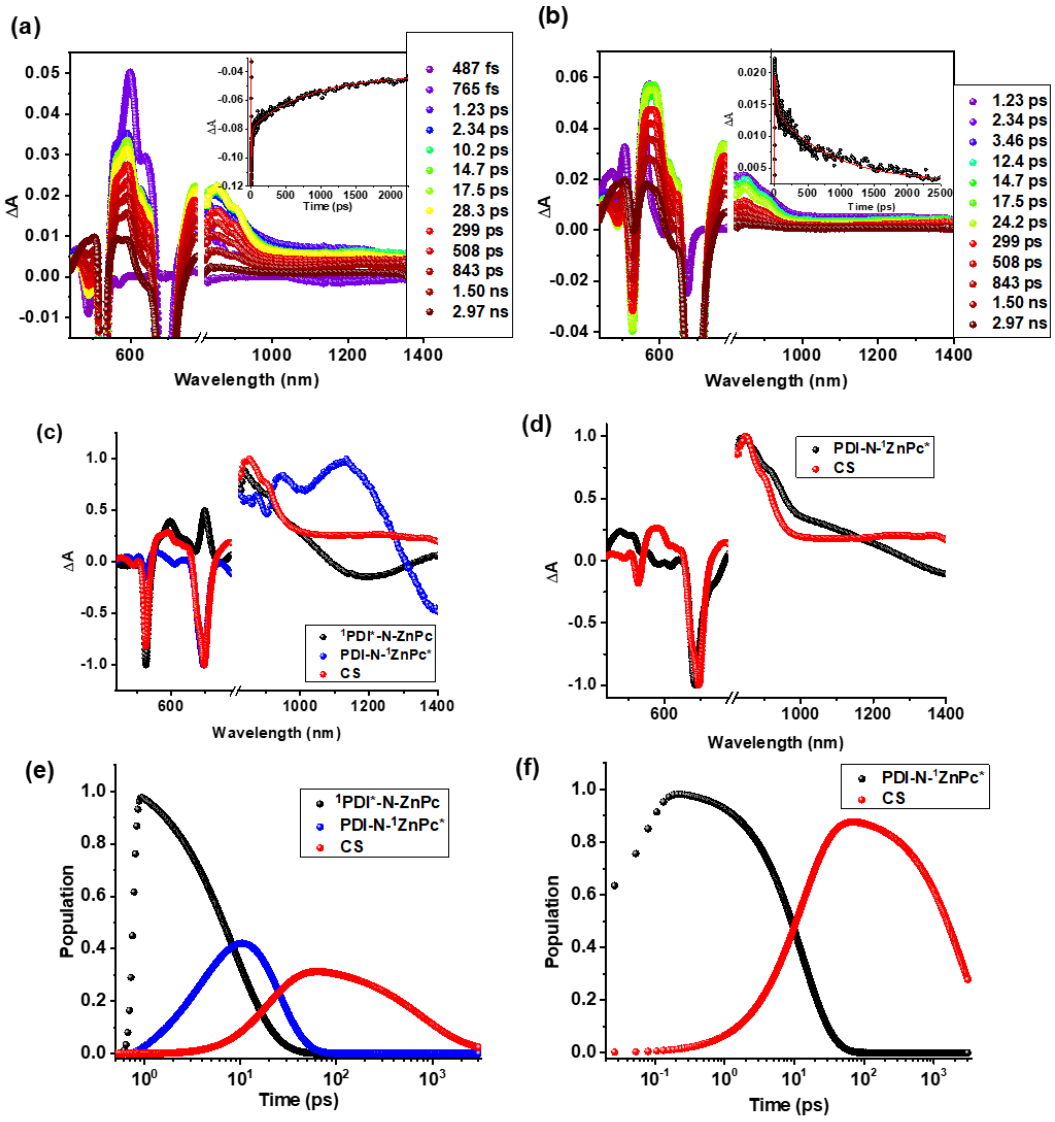

Figure 7. Fs-TA spectra in toluene at the indicated delay times of **PDI-N-ZnPc** dyad (a) excited at 530 nm, and (b) excited at 680 nm. The evolution-associated spectra (EAS) and population kinetics from GloTarAn analysis for dyad excited at (c and e) 530 nm and (d and f) 680 nm are shown below. The insets in (a) and (b) show the time profiles of the 687 and 843 nm peaks for the dyad, respectively.

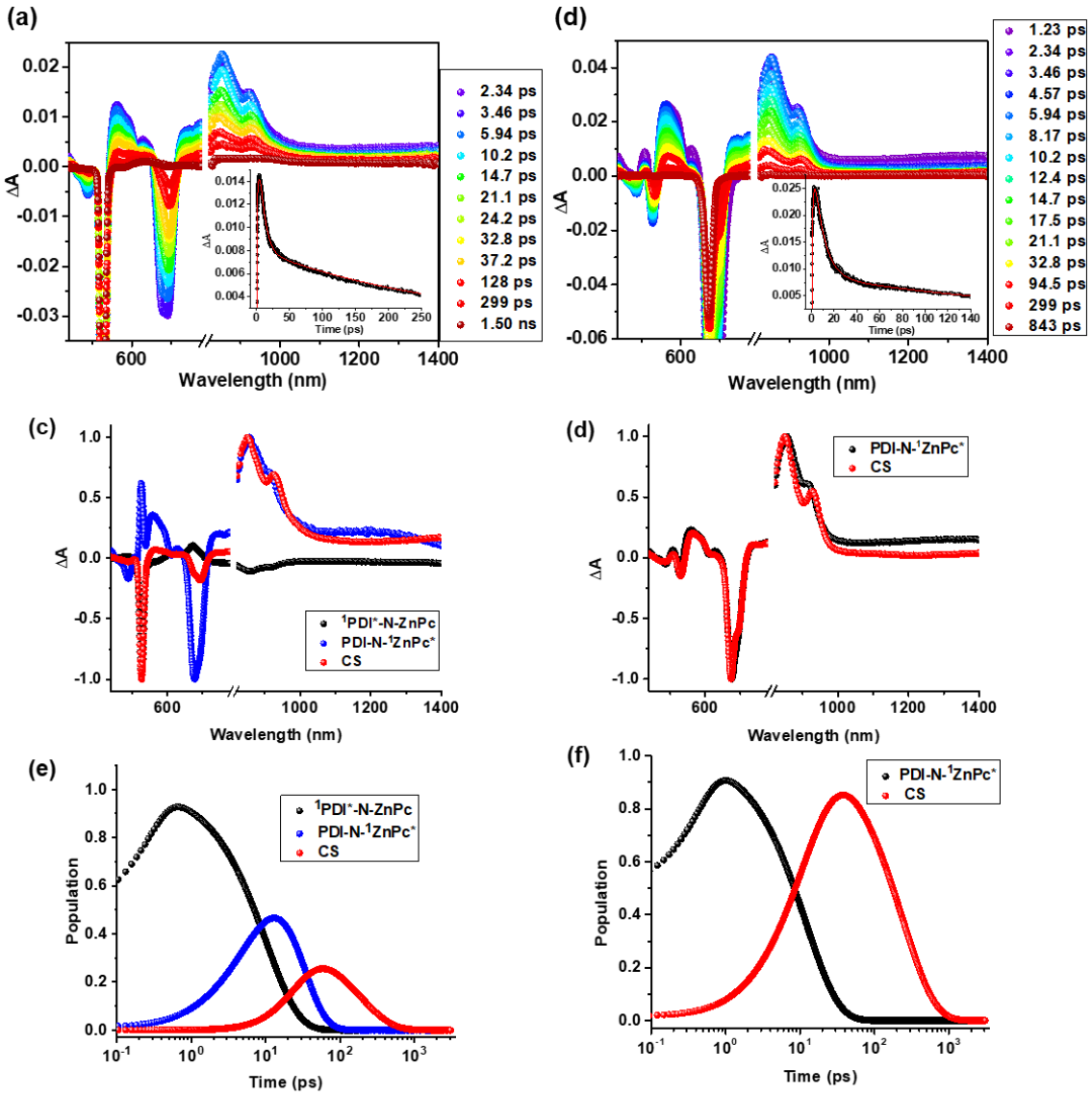

Figure 8. Fs-TA spectra in benzonitrile at the indicated delay times of **PDI-N-ZnPc** dyad (a) excited at 530 nm, and (b) excited at 680 nm. The evolution-associated spectra (EAS) and population kinetics from GloTarAn analysis for dyad excited at (c and e) 530 nm and (d and f) 680 nm are shown below. The insets in (a) and (b) show the time profiles of the 932 and 925 nm peaks for the dyad, respectively.

The GloTarAn analyzed time constants are given in Table 1 for singlet-singlet energy transfer (EnT), charge separation (CS), and charge recombination (CR). In contrast to the previously reported **Dyad 1** and **2**, the current **PDI-N-ZnPc** achieved a favorable balance between efficient charge separation and suppressed recombination. While **Dyad 1** revealed ultrafast energy transfer <1.00 ps in toluene, its charge separation persisted 33.3 ps and recombination was longer (244 ps), leading to the persistence of the charge-separated (CS) state. With a more twisted geometry, **Dyad 2** showed rapid CS of 11.0 ps but relatively long-lasting recombination (605 ps). On the other hand, **PDI-N-ZnPc** yielded a relatively longer-lived CS state through integrating the efficient

charge separation (11.16 ps) with the prolonged recombination (752.26 ps). Among all three conjugates **PDI-N-ZnPc** showed enhanced CS in polar benzonitrile, and sustained the slowest rate of CR, allowing for a long-lived CS state that lasts up to 187.17 ps. Upon stimulation at 680 nm, the trend continued with **PDI-N-ZnPc** exhibiting long-lasting recombination while retaining acceptable CS time constant. Overall, the optimized geometry and orbital separation of N-linked dyad enable prolonged CS lifetime, surpassing previous designs in both solvents.

Table 1. Time constants for the energy and electron transfer processes from fs-TA studies in the studied dyads in toluene and benzonitrile from GloTarAn analysis. (estimated error= +10%).

λ_{ex} nm	Solvent	**PDI-N-ZnPc**			**Dyad 1**[11]			**Dyad 2**[11]		
		EnT [ps]	CS [ps]	CR [ps]	EnT [ps]	CS [ps]	CR [ps]	EnT [ps]	CS [ps]	CR [ps]
530	TOL	8.44	11.16	752.26	<1	33.3	244	<1	11.0	605
	PhCN	11.12	13.80	187.17	12.6	0.60	23.1	16.1	1.00	9.60
680	TOL	-	11.77	$2.93x10^3$	-	22.6	280.7	-	8.77	656
	PhCN	-	13.46	251.49	-	1.60	7.40	-	1.30	5.50

Abbreviations: Toluene = TOL, Benzonitrile = PhCN

Conclusions

In summary, several intriguing results have emerged from the current study on a newly synthesized **PDI-N-ZnPc** conjugate linked via an N-pyrrolic bridge. Significant yields of N-linked conjugate were obtained using the synthetic procedures outlined here. The spectral and redox potentials have been affected by intramolecular interactions owing to the proximity caused by the reduced R_{cc} and enhanced orbital overlap of the donor and acceptor entities. While interacting with electron-deficient PDI, ZnPc exhibited anodically shifted oxidation and spectral broadening with near continuous light absorption across the 300–750 nm range. DFT studies identified donor and acceptor entities that were nearly coplanar, with a LUMO on PDI and a HOMO on ZnPc in optimized geometries. Comparatively lower dihedral angles in **PDI-N-ZnPc** than those of **Dyad 1** and **2** improved the orbital overlap while maintaining the electronic asymmetry. The formation of $(PDI\text{-}N)^{\bullet-}$-$ZnPc^{\bullet+}$ CS state upon excitation of ZnPc in the dyads was confirmed based on the transient absorption experiments conducted at various excitation wavelengths in toluene and benzonitrile. However, the ultrafast energy transfer and subsequent electron transfer of the N-linked conjugate in both solvents were revealed by the selective excitation of PDI. Overall, the **PDI-N-ZnPc** dyad exhibited excellent control over charge-transfer kinetics, attaining balanced excitation transfer and charge separation with minimized recombination. These results validate the structural strategy of the novel N-linked dyad, allowing it to outperform previous constructs in

sustaining long-lived charge-separated states. Together, these properties make **PDI-N-ZnPc** a promising molecular design for artificial photosynthesis, photoconversion, and photocatalytic applications, which may be used in designing broadband-capturing solar and optoelectronic devices.

Acknowledgments

This work was supported by the National Science Foundation (2345836 and 2514911 to FD). We also acknowledge Grant PID2022-140315NB-I00 (to F.F.-L.) funded by MICIU/AEI/10.13039/501100011033 and by ERDF/EU, and Grant PID2024-155430OB-I00 (to Á.S.-S) funded by the European Regional Development Fund "A way to make Europe" and the Spanish Ministerio de Ciencia e Innovación/Agencia Estatal de Investigación. F.F.-L. and Á.S.-S. are also indebted to Generalitat Valenciana (CIPROM/2021/059) and the Advanced Materials program by MCIN with funding from European Union NextGenerationEU (PRTR-C17.I1) and Generalitat Valenciana (MFA/2022/ 028). Additional NSF support for the UNT CASCaM HPC cluster via Grant CHE-1531468 is also gratefully acknowledged.

References

[1] M. R. Wasielewski, "Photoinduced electron transfer in supramolecular systems for artificial photosynthesis." *Chem. Rev.* **1992***, 92*, 435–461.

[2] S. Fukuzumi, H. Kotani, K. Ohkubo, S. Ogo, N. V. Tkachenko, H. Lemmetyinen, "Electron-transfer state of 9-mesityl-10-methylacridinium ion with a much longer lifetime and higher energy than that of the natural photosynthetic reaction center" *J Am Chem Soc.* **2004,** *126*,1600-1601. DOI: 10.1021/ja038656q.

[3] H. Imahori, T. Umeyama, S. Ito, "Large π-Aromatic Molecules as Potential Sensitizers for Highly Efficient Dye-Sensitized Solar Cells" *Acc. Chem. Res.* **2009**, *42*, 1809–1818.

[4] B. Sekaran, A. Dawson, Y. Jang, K. V. MohanSingh, R. Misra, F. D'Souza, "Charge-Transfer in Panchromatic Porphyrin-Tetracyanobuta-1,3-Diene-Donor Conjugates: Switching the Role of Porphyrin in the Charge Separation Process" *Chem. Eur. J.* **2021**, *27*, 14335-14344.

[5] F. D'Souza, V. Krishnan, "Intramolecular Donor-Acceptor Systems: Structures Of Novel Linked Porphyrin- Phenolphthalein Molecular Systems" *J. Photochem. Photobiol.* **1990**, *51*, 285-291.

[6] A. Benitz, M. B. Thomas, F. D'Souza, "Geometry-Controlled Photoinduced Charge Separation and Recombination in a Trans-A_2B_2-Functionalized Donor–Acceptor Conjugate Composed of a Multimodular Zinc Porphyrin and Fullerene" *ChemPhotoChem* **2017**, *1*, 17.

[7] A. Moss, Y. Jang, J. Arvidson, H. Wang, F. D'Souza, "Highly Coupled Heterobicycle-Fused Porphyrin Dimers: Excitonic Coupling and Charge Separation with Coordinated Fullerene, C_{60}" *ChemSusChem* **2023**, *16*, e202202289.

[8] M. Guragain, D. Pinjari, R. Misra, F. D'Souza, "Zinc Tetrapyrrole Coordinated to Imidazole Functionalized Tetracyanobutadiene or Cyclohexa-2,5-diene-1,4-diylidene-

expanded-tetracyanobutadiene Conjugates: Dark vs. Light-Induced Electron Transfer" *Chem. Eur. J.* **2023**, *29*, e202302665.

[9] R. Marczak, K. Nowakowski, W. Kutner, B. Desbat, Y. Araki, O. Ito, S. Gadde, M. E. Zandler, F. D'Souza, "Self-Assembling of Porphyrin-Fullerene Dyads in the Langmuir and Langmuir-Blodgett Films: Formation as well as Spectral, Electrochemical and Vectorial Electron Transfer Studies" *J. Nanosci. Nanotechnol.* **2007**, *7*, 1455-1471.

[10] S. Washburn, R. R. Kaswan, S. Shaikh, A. Moss, F. D'Souza, H. Wang, "Excited-State Charge Transfer in Push–Pull Platinum(II) π-Extended Porphyrins Fused with Pentacenequinone" *J. Phys. Chem. A* **2023**, *127*, 9040-9051.

[11] N. Zink-Lorre, E. Font-Sanchis, S. Seetharaman, P. A. Karr, Á. Sastre-Santos, F. D'Souza, F. Fernández-Lázaro, "Directly Linked Zinc Phthalocyanine–Perylenediimide Dyads and a Triad for Ultrafast Charge Separation." *Chem. Eur. J.* **2019**, *25*, 10123-10132.

[12] F. D'Souza, E. Maligaspe, K. Ohkubo, M. E. Zandler, N. K. Subbaiyan, S. Fukuzumi, "Photosynthetic Reaction Center Mimicry: Low Reorganization Energy Driven Charge Stabilization in Self-Assembled Cofacial Zinc Phthalocyanine Dimer−Fullerene Conjugate" *J. Am. Chem. Soc.* **2009**, *131*, 8787-8797.

[13] L. M. Arellano, H. B. Gobeze, Y. Jang, M. Barrejón, C. Parejo, J. C. Álvarez, M. J. Gómez-Escalonilla, Á. Sastre-Santos, F. D'Souza, F. Langa, "Formation and Photoinduced Electron Transfer in Porphyrin- and Phthalocyanine-Bearing N-Doped Graphene Hybrids Synthesized by Click Chemistry" *Chem. Eur. J.* **2022**, *28*, e202200254.

[14] C. B. KC, G. N. Lim, F. D'Souza, "Multi-modular, tris(triphenylamine) zinc porphyrin–zinc phthalocyanine–fullerene conjugate as a broadband capturing, charge stabilizing, photosynthetic 'antenna-reaction center' mimic." *Nanoscale* **2015***, 7*, 6813–6826.

[15] C. B. KC, G. N. Lim, P. A. Karr, F. D'Souza, "Supramolecular Tetrad Featuring Covalently Linked Bis(porphyrin)–Phthalocyanine Coordinated to Fullerene: Construction and Photochemical Studies." *Chem. Eur. J.* **2014**, *20*, 7725-7735.

[16] S Das, P. K. Gupta, R. Misra, F. D'Souza, "Acceptor-Dependent Intervalence Charge Transfer and Separation Dynamics in Broad-Band-Capturing Push–Pull Chromophores." *J. Phys. Chem. C* **2025***, 129*, 6924–6942.

[17] F. Würthner, T. E. Kaiser, C. R. Saha-Möller, "J-Aggregates: From Serendipitous Discovery to Supramolecular Engineering of Functional Dye Materials" *Angew. Chem. Int. Ed.* **2011**, *50*, 3376–3410.

[18] G. Bottari, G. de la Torre, D. M. Guldi, T. Torres, "Covalent and Noncovalent Phthalocyanine−Carbon Nanostructure Systems: Synthesis, Photoinduced Electron Transfer, and Application to Molecular Photovoltaics" *Chem. Rev.* **2010**, *110*, 6768-6816.

[19] G. L. Closs, J. R. Miller, "Intramolecular long-distance electron transfer in organic molecules." *Science* **1988**, *240,* 440-447. DOI: 10.1126/science.240.4851.440.

[20] S. Seetharaman, Y. Jang, C. B. KC, P. A. Karr, F. D'Souza, "Peripheral phenothiazine induced suppression of charge separation from the singlet excited zinc phthalocyanine to coordinated C_{60} in supramolecular donor–acceptor conjugates." *J. Porphyrins Phthalocyanines* **2017***, 21*, 870–881.

[21] D. Wöhrle, in *Phthalocyanines: Properties and applications, Vol. 1* (Eds.: C. C. Leznoff, A. B. P. Lever), VCH, Weinheim, **1989**, 436.

[22] F. Würthner, "Perylene bisimide dyes as versatile building blocks for functional supramolecular architectures." *Chem. Commun.* **2004**, 1564–1579.

[23] H. Xu, J. Zhang, X. Qiao, L. Ding, A. Wang, H. Liu, X. Yu, "Recent research progress on perylene diimide-based photocatalytic materials." *Fundamental Research* **2025**.
[24] K. T. Cho, K. Rakstys, M. Cavazzini, S. Orlandi, G. Pozzi, M. K. Nazeeruddin, "Perovskite Solar Cells Employing Molecularly Engineered Zn(II) Phthalocyanines as Hole-transporting Materials." *Nano Energy* **2016***, 30*, 853–857.
[25] Z. Ma, H. Fu, D. Meng, W. Jiang, Y. Sun, Z. Wang, "Isomeric N-Annulated Perylene Diimide Dimers for Organic Solar Cells." *Chem. Asian J.* **2018**, *13*, 918-923. DOI: 10.1002/asia.201800058.
[26] E. M. Maya, P. Vázquez, T. Torres, "Synthesis of Alkynyl-Linked Phthalocyanine Dyads: Push–Pull Homo- and Heterodimetallic Bisphthalocyaninato Complexes." *Chem. Eur. J.* **1999**, *5*, 2004-2013.
[27] M. Gassara, J. Garcés-Garcés, L. Lezema, J. Ortiz, F. Fernández-Lázaro, S. Kazim, Á. Sastre-Santos, S. J. Ahmad, "Dopant-free tert-butyl Zn(ii) phthalocyanines: the impact of substitution on their photophysical properties and their role in perovskite solar cells." *Mater. Chem. C*. **2025**, *13*, 1704-1721.
[28] A. M. Gutiérrez-Vílchez, C. V. Ileperuma, V. Navarro-Pérez, P. A. Karr, F. Fernández-Lázaro, F. D'Souza, "Excited Charge Transfer Promoted Electron Transfer in all Perylenediimide Derived, Wide-Band Capturing Conjugates: A Mimicry of the Early Events of Natural Photosynthesis" *ChemPlusChem* **2024**, *89*, e202400348.
[29] A. Nowak-Król, F. Würthner, "Progress in the synthesis of perylene bisimide dyes." *Org. Chem. Front.* **2019***, 6*, 1272–1318.
[30] A. Nowak-Król, K. Shoyama, M. Stolte, F. Würthner, "Naphthalene and perylene diimides – better alternatives to fullerenes for organic electronics?" *Chem. Commun.* **2018***, 54*, 13763–13772.
[31] M. Ball, B. Zhang, Y. Zhong, B. Fowler, S. Xiao, F. Ng, M. Steigerwald, C. Nuckolls, "Conjugated Macrocycles in Organic Electronics." *Acc. Chem. Res.* **2019***, 52*, 1068–1078.
[32] V. Navarro-Pérez, A. M. Gutiérrez-Vílchez, J. Ortiz, J.; Á. Sastre-Santos, F. Fernández-Lázaro, S. Seetharaman, M. J. Duffy, P. A. Karr, F. D'Souza, "A zinc phthalocyanine–benzoperylenetriimide conjugate for solvent dependent ultrafast energy vs. electron transfer." *Chem. Commun.* **2019***, 55*, 14946–14949.
[33] J. R. Lakowicz, *Principles of Fluorescence Spectroscopy*, 3rd ed., Springer, Singapore, 2006.
[34] E. Maligaspe, T. Kumpulainen, H. Lemmetyinen, N. V. Tkachenko, N. K. Subbaiyan, M. E. Zandler, F. D'Souza, "Ultrafast singlet-singlet energy transfer in self-assembled via metal-ligand axial coordination of free-base porphyrin-zinc phthalocyanine and free-base porphyrin-zinc naphthalocyanine dyads" *J. Phys. Chem. A* **2010**, *114*, 268–277.
[35] G. N. Lim, E. Maligaspe, M. E. Zandler, F. D'Souza, "A Supramolecular Tetrad Featuring Covalently Linked Ferrocene–Zinc Porphyrin–BODIPY Coordinated to Fullerene: A Charge Stabilizing, Photosynthetic Antenna–Reaction Center Mimic" *Chem. Eur. J.* **2014**, *20*, 17089–17099.
[36] D. Gust, T. A. Moore, A. L. Moore, "Mimicking Photosynthetic Solar Energy Transduction" *Acc. Chem. Res.* **2009**, *42*, 1890–1898.
[37] J. N. Clifford, G. Accorsi, F. Cardinali, J. F. Nierengarten, N. Armaroli, "Photoinduced electron and energy transfer processes in fullerene C_{60}–metal complex hybrid assemblies" *C. R. Chim.* **2006**, *9*, 1005–1013.

[38] N. Martín, L. Sánchez, M. A. Herranz, B. Illescas, D. M. Guldi, "Electronic Communication in Tetrathiafulvalene (TTF)/C_{60} Systems: Toward Molecular Solar Energy Conversion Materials?" *Acc. Chem. Res.* **2007**, *40*, 1015–1024.

[39] M. El-Khouly, S. Fukuzumi, F. D′Souza, "Photosynthetic antenna-reaction center mimicry by using boron dipyrromethene sensitizers." *ChemPhysChem* **2014**, *15*, 30–47.

[40] C. V. Ileperuma, J. Garcés-Garcés, S. Shao, F. Fernández-Lázaro, Á. Sastre-Santos, P. A. Karr, F. D'Souza, "Panchromatic Light-Capturing Bis-styryl BODIPYPerylenediimide Donor-Acceptor Constructs: Occurrence of Sequential Energy Transfer Followed by Electron Transfer" *Chem. Eur. J.* **2023**, *29*, e202301686.

[41] M. A. Dahlen, "The Phthalocyanines A New Class of Synthetic Pigments and Dyes." *Ind. Eng. Chem.* **1939**, *31*, 839–847.

[42] K. M. Kadish, K. M. Smith, R. Guilard (Eds.), *The Porphyrin Handbook, Vol. 16*, Academic Press, San Diego, **2003**.

[43] *Gaussian 16*, Revision C.A03, M. J. Frisch, G. W. Trucks, H. B. Schlegel, G. E. Scuseria, M. A. Robb, J. R. Cheeseman, G. Scalmani, V. Barone, B. Mennucci, G. A. Petersson, H. Nakatsuji, M. Caricato, X. Li, H. P. Hratchian, A. F. Izmaylov, J. Bloino, G. Zheng, J. L. Sonnenberg, M. Hada, M. Ehara, K. Toyota, R. Fukuda, J. Hasegawa, M. Ishida, T. Nakajima, Y. Honda, O. Kitao, H. Nakai, T. Vreven, J. A., Jr., Montgomery, J. E. Peralta, F. Ogliaro, M. Bearpark, J. J. Heyd, E. Brothers, K. N. Kudin, V. N. Staroverov, R. Kobayashi, J. Normand, K. Raghavachari, A. Rendell, J. C. Burant, S. S. Iyengar, J. Tomasi, M. Cossi, N. Rega, J. M. Millam, M. Klene, J. E. Knox, J. B. Cross, V. Bakken, C. Adamo, J. Jaramillo, R. Gomperts, R. E. Stratmann, O. Yazyev, A. J. Austin, R. Cammi, C. Pomelli, J. W. Ochterski, R. L. Martin, K. Morokuma, V. G. Zakrzewski, G. A. Voth, P. Salvador, J. J. Dannenberg, S. Dapprich, A. D. Daniels, Ö. Farkas, J. B. Foresman, J. V. Ortiz, J. Cioslowski, D. J. Fox, Gaussian, Inc., Wallingford, CT, USA, 2016.

[44] *GaussView*, Version 6.0.16, Roy Dennington, Todd A. Keith, John M. Millam, Semichem Inc., Shawnee Mission, KS, 2016

[45] R. R. Kaswan, S. Washburn, U. Oji, H. Wang, F. D'Souza, "Directly Fused Porphyrin-Tetracyanopentacenequinone Conjugates: Role of the Cross-Conjugated, Powerful Electron Acceptor in Promoting Highly Efficient Charge Separation" *Chem. - Eur. J.* **2025**, *31*, e202404165 (1-12).

[46] M. Wazid, Y. Rout, A. Z. Alsaleh, R. R. Kaswan, R. Misra, F. D'Souza, "Perylenediimide promoted charge transfer in tetracyano butadiene–triphenylamine (TCBD–TPA) and expanded-tetracyano butadiene–triphenylamine (DCNQ–TPA) push–pull conjugates" *Chem. Commun*. **2025**, *61*, 6803-6806.

[47] J. K. Sharma, D. R. Subedi, P. A. Karr, F. D'Souza, "Nickel porphyrin-C_{60} dyads: Significance of low-lying porphyrin orbitals to suppress excited charge and energy transfer" *J. Porphyrins Phthalocyanines* **2025**, *29*, 354-366.

[48] P. K. Gupta, C. V. Ileperuma, R. Misra, F. D'Souza, "Strong acceptor incorporated phenothiazine-C_{60} multi-redox push–pull conjugates: demonstration of C_{60}'s superior electron acceptor characteristics" *Chem. Sci*. **2025**, *16*, 12122-12128.

[49] A. W. Dawson, B. Sekaran, S. Das, R. Misra, F. D'Souza, "Synthesis and Understanding of the Role of Donor-Tetracyanobutadiene in Porphyrin β-Periphery toward Ultrafast Charge Transfer Dynamics." *J. Phys. Chem. C* **2024***, 128*, 18857–18871.

[50] D. Rehm, A. Weller, " Kinetics of Fluorescence Quenching by Electron and H-Atom Transfer." *Isr. J. Chem.* **1970**, *8*, 259–271.

[51] Y. Hou, X. Zhang, K. Chen, D. Liu, Z. Wang, Q. Liu, J. Zhao, A. Barbon, "Charge separation, charge recombination, long-lived charge transfer state formation and intersystem crossing in organic electron donor/acceptor dyads." *J. Mater. Chem. C* **2019***, 7*, 12048–12074.

[52] R. R. Kaswan, D. Molina, L. Ferrer-López, J. Ortiz, P. A. Karr, Á. Sastre-Santos, F. D'Souza, "Intervalence Charge Transfer and Exothermic and Isoenergetic Symmetry Breaking Charge Separation in Far-Red Capturing Zinc Phthalocyanine Dimers" *Angew. Chem. Int. Ed.* **2025**, *64*, e202502516.

[53] I. H. M. van Stokkum, D. S. Larsen, R. Grondelle, "Global and target analysis of time-resolved spectra." *Biochim Biophys Acta.* **2004**, *1657*, 82-104.

[54] J. J. Snellenburg, S. P. Laptenok, R. Seger, K. M. Mullen, I. H. M. van Stokkum, "Glotaran: A Java-Based Graphical User Interface for the R Package TIMP" *J. Stat. Softw.* **2012**, *49*, 1–22.

[55] I. H. M. van Stokkum, J. Ravensbergen, J. J. Snellenburg, R. van Grondelle, S. Pillai, T. A. Moore, D. Gust, A. L. Moore, J.T.M. Kennis. In Robert B, ed. *Advances in Botanical Research. Vol 79. Artificial Photosynthesis*. Academic Press, 2016; 169-192.

[56] http://glotaran.org/

Entry for the Table of Contents

Zinc Phthalocyanine N-Linked to Pyrroloperylenediimide Dyad: Significance of N-Connectivity in Modulating Photodynamics Towards Prolonging the Lifetime of Charge Separation

C. V. Ileperuma, J. Garcés-Garcés, A. M. Gutiérrez-Vílchez, Á. Sastre-Santos, F. Fernández Lázaro*, and F. D'Souza*

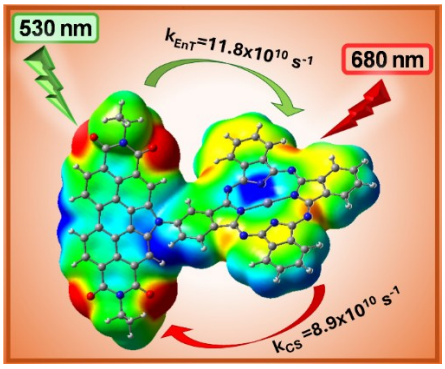

The newly synthesized zinc phthalocyanine-pyrroloperylenediimide dyad connected through a nitrogen heteroatom **(PDI-N-ZnPc)** has been shown to undergo solvent polarity-dependent singlet-singlet energy transfer and electron transfer. The persistence of the electron transfer product, compared to earlier reported dyads in this series, is demonstrated through femtosecond transient absorption studies.